

# *Ab initio* structure determination using dispersive differences from multiple-wavelength synchrotron-radiation powder diffraction data

John R. Helliwell,<sup>a\*</sup> Madeleine Helliwell<sup>a</sup> and Richard H. Jones<sup>b</sup><sup>a</sup>Department of Chemistry, The University of Manchester, Manchester M13 9PL, England, and<sup>b</sup>Lennard-Jones Laboratories, School of Chemistry and Physics, Keele University, Keele,

Staffordshire ST5 5BG, England. Correspondence e-mail: john.helliwell@manchester.ac.uk

The purpose of this paper and a test case study is to assess a method of *ab initio* structure solution from powder diffraction data using  $f'$  difference techniques. A theoretical foundation for the approach used is first provided. Then, with a test case (nickel sulfate hexahydrate), it is shown that both the position of the anomalous scatterer (Ni) can be determined and the structure can be developed in full. Specifically, synchrotron-radiation data were collected at two wavelengths close to the *K* edge for Ni and three wavelengths remote from the Ni absorption edge, at 1.3, 1.8 and 2.16 Å. These five wavelengths then allowed various combinations to be tried to establish which wavelength pairs gave the optimum signal in the Patterson maps using dispersive amplitude differences. The initial phases derived from the metal-atom position then allowed the structure to be fully developed by difference Fourier cycling. The relevance of these developments to structure-solution possibilities for proteins *via* powder dispersive difference data is then outlined.

© 2005 International Union of Crystallography  
Printed in Great Britain – all rights reserved

## 1. Introduction

Various advances have been made in the field of *ab initio* structure solution from powder diffraction data. One significant advance in the last two decades involves instrumentation for the use of finely collimated synchrotron radiation where better resolved powder lines have been found to be beneficial in the structure solution of, for example, cimetidine (Cernik *et al.*, 1991). A different method involving the use of variable temperature measurements to exploit anisotropic thermal expansion also reduced the peak-to-peak overlap (Shankland, David & Sivia, 1997). There have in addition been advances in structure-solution methodology with powder data, *e.g.* use of Monte Carlo methods (Harris *et al.*, 1994; Tremayne *et al.*, 1997), simulated annealing (David *et al.*, 1998; Pagola & Stephens, 2000) and genetic algorithms (Shankland, David & Csoka, 1997; Kariuki *et al.*, 1997). Despite these advances, *ab initio* structure solution from powder diffraction data is still not routine, particularly for more complex structures; this is because, generally, there are a significant number of overlapping reflections, in addition to the fact that Friedel pairs of reflections are exactly coincident. Thus, there tends to be an underdetermination of data, somewhat similar to that seen in macromolecular crystallography, where the data tend to be weak and therefore do not routinely extend to atomic resolution. Indeed, powder dispersive differences (PDD) may be of important application in protein powder diffraction, which we explain.

The so called multiple-wavelength anomalous-dispersion (MAD) method is now routinely employed for the crystal structure solution of macromolecules. This exploits the changes in the atomic scattering factor that take place close to the absorption edges of elements, owing to the variation of  $f'$  and  $f''$  with wavelength, where the atomic scattering factor is given by

$$f = f^0 + f'(\lambda) + if''(\lambda)$$

and  $f^0$  is the basic scattering factor of an atom and  $f'(\lambda)$  and  $f''(\lambda)$  are its real and imaginary components of the anomalous scattering. By tuning to the absorption edge of a specific element in a sample to stimulate the maximum changes in  $f'$ , it is possible to induce differences in reflection intensities with wavelength, similar to those seen with the isomorphous replacement method [see *e.g.* Helliwell (1992) and Ramakrishnan & Biou (1997) for such a treatment]. Approximately a third of all genes are thought to code for metalloproteins, thus providing an anomalous scatterer in these cases. Alternatively, selenomethionine substitution affords a protein production method, which has general utility for MAD *via* the Se *K* edge (Hendrickson *et al.*, 1990).

In the powder diffraction field, Mitchell (1957), working from Okaya & Pepinsky (1956), derived a two-wavelength anomalous-dispersion formalism for use in crystal structure analysis and also mentioned its application to powder diffraction. Anomalous difference powder methods have been used to provide a quantitative and qualitative analysis of

Co<sub>3</sub>O<sub>4</sub> in the matrix of kaolinite [Al<sub>2</sub>Si<sub>2</sub>O<sub>5</sub>(OH)<sub>4</sub>], using laboratory-based data measured at Co *Kα* and *Kβ* wavelengths (Wood *et al.*, 1986). Prandl (1990, 1994) suggested a difference method using partial Patterson densities, rather than the more basic dispersive difference Patterson densities, for *ab initio* structure solution from powder diffraction data, which was tested for SrSO<sub>4</sub> (Burger *et al.*, 1998). Gu *et al.* (2000) used simulated two-wavelength X-ray powder data for C<sub>14</sub>H<sub>20</sub>O<sub>2</sub>N<sub>2</sub>·HBr and direct methods to break the phase ambiguity; they compared the effectiveness of developing the rest of the structure after finding the anomalous scatterer (Br) atom by their direct method *versus* conventional difference Fourier cycling; a reduction in the number of iterations by a factor of two was observed.

We offer in this paper some different approaches for the PDD case.

(i) We provide a theoretical basis derived from protein crystallography, specifically working from Helliwell (1992) to locate the anomalous-scatterer positions.

(ii) More generally, the peak-to-peak overlap is relieved by working initially (for structure solution) with data truncated in resolution limit for both full and difference powder diffraction patterns.

(iii) Additionally, general relief of the peak-to-peak overlap problem for the full pattern is available *via* use of softer X-rays which spreads out the lines. A wavelength as soft as 1.8 or even 2 Å would still allow, in full back-scattering mode, diffraction data to 0.9 or 1 Å, respectively, to be recordable. This is tested here. A different, more extreme, example of powder diffraction using soft, 5 Å, X-rays is described by Cernik *et al.* (2005).

(iv) Our study also affords an investigation of which wavelength pairs in our experiment lead to optimal PDD results.

(v) Overall, PDD techniques could be employed to extract the signal from the anomalously scattering atom of interest, locating the atom using the Patterson method from dispersive differences and using that as the initial phase information. Like the heavy-atom method in single-crystal work, the rest of the structure could be determined by difference Fourier techniques to locate the non-anomalously scattering atoms.

(vi) The development of PDD is relevant to protein crystal powder diffraction. It has been shown by Von Dreele *et al.* (2000) and Margiolaki *et al.* (2005) that protein model refinement and molecular replacement structure solution are possible with protein powder data. However, structure solution from PDD data has potential too; there is the complication, however, compared with the standard protein crystallography MAD method that, since  $F(hkl)$  and  $F(\overline{h}\overline{k}\overline{l})$  are exactly overlapped in powder patterns, there will be a phase ambiguity (see Fig. 9.11 in Helliwell, 1992). The phase ambiguity for each reflection would have to be resolved *via* other information such as by calculating a map using averaged phases and using *e.g.* solvent flattening to improve the reflection phase estimations.

This paper and test case study provides a foundation for PDD applicable to many absorption edges, to inorganics and to proteins containing metals or selenomethionine or xenon introduced under high pressure.

## 2. Theoretical foundation for this paper

Using Fig. 1 and the cosine rule, we have the following equation:

$$F_{LH\lambda_1}^2 = F_{LH\lambda_2}^2 + \Delta f'^2 - 2F_{LH\lambda_2} \Delta f' \cos[\pi - (\alpha_{LH\lambda_2} - \alpha_H)], \quad (1)$$

where L refers to the combined scattering of the light-atom (non-anomalous) scatterers, H refers to the heavy-atom scattering (anomalous scatterer), LH refers to the resultant scattering of the light and heavy atoms, and the two wavelengths used are  $\lambda_1$  and  $\lambda_2$ .  $\Delta f'$  is the difference, as a vector for the given reflection, due to the two different  $f'$  values of the anomalous scatterer between these two wavelengths. Finally,  $\alpha_{LH\lambda_2}$  and  $\alpha_H$  are the phase angles of the structure factors of the light and heavy atoms at wavelength 2 and the heavy atoms alone, respectively. Note that Fig. 1 is showing vector quantities but in the derivation here we refer to the amplitudes of those vector quantities.

We rearrange (1) as follows:

$$F_{LH\lambda_2}^2 - F_{LH\lambda_1}^2 + \Delta f'^2 = 2F_{LH\lambda_2} \Delta f' \cos[\pi - (\alpha_{LH\lambda_2} - \alpha_H)]. \quad (2)$$

This is

$$(F_{LH\lambda_2} + F_{LH\lambda_1})(F_{LH\lambda_2} - F_{LH\lambda_1}) + \Delta f'^2 = 2F_{LH\lambda_2} \Delta f' \cos[\pi - (\alpha_{LH\lambda_2} - \alpha_H)]. \quad (3)$$

Since the purpose of our paper is to address the situation of extending powder methods to larger unit cells and correspondingly larger structures, it is likely that most of the cases

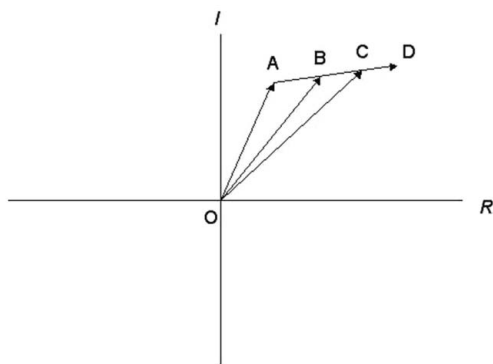


Figure 1

Argand diagram showing the contribution of light atoms  $F_L$  and the normal scattering of the anomalous-scatterer atoms  $F_{Ho}$  with a stimulated wavelength dispersive effect  $\Delta f'$ . Point B represents an average of the Friedel reflection pairs at  $\lambda_2$ ,  $F_{LH\lambda_2}^+$  and  $F_{LH\lambda_2}^-$ , and likewise for point C at  $\lambda_1$ , owing to the superposition of Friedel reflections in powder diffraction data. The angles  $\alpha_{LH\lambda_2}$  and  $\alpha_H$  are respectively the angles between the real axis and OB for the former and the real axis and AD for the latter. Then,  $OA = F_L$ ,  $DC = f'_{\lambda_1}$ ,  $DB = f'_{\lambda_2}$ ,  $AD = F_{Ho}$ ,  $CB = \Delta f'_{\lambda_2-\lambda_1}$ ,  $OB = F_{LH\lambda_2}$ ,  $OC = F_{LH\lambda_1}$ .

will involve a relatively large number of light atoms. Hence we can make the approximation to (3) for the majority of the cases that

$$\Delta f'^2 \ll (F_{LH\lambda_2} + F_{LH\lambda_1})(F_{LH\lambda_2} - F_{LH\lambda_1}). \quad (4)$$

Also,

$$(F_{LH\lambda_2} + F_{LH\lambda_1}) \approx 2F_{LH\lambda_2} \quad (5)$$

and (3) thus becomes

$$(F_{LH\lambda_2} - F_{LH\lambda_1}) \approx \Delta f' \cos[\pi - (\alpha_{LH\lambda_2} - \alpha_H)]. \quad (6)$$

Equation (6) shows that the measured structure-factor amplitudes at each wavelength when subtracted one from the other produces a signal that, in our approximation, is derived from the anomalously scattering atom alone. We see in the analysis section below that, even in the case here of one Ni atom in the presence of just 11 light atoms, the Patterson function calculated with coefficients that are the left-hand side of equation (6) shows predominantly Ni-atom self-vectors. Prandl (1990, 1994) gives the exact treatment, where he shows that use of 'simple' differences in a Patterson synthesis, *i.e.*  $(F_{LH\lambda_2} - F_{LH\lambda_1})^2$  also yields cross vectors between the H and L atoms; this is also evident from the right-hand sides of equations (1)–(3).

The above treatment can be trivially extended first to the case of more than one anomalously scattering atom of the same type. In such a case,  $\Delta f'$  in the above equations is a combined vector, which is the collective effect of the several atoms. This is similar to  $F_L$  being a vector combined from the vector contributions of each and every light atom. The extension to the case of more than one anomalously scattering atom type, whether of one or more atoms in each case, is non-trivial only in as much as the two wavelengths aiming to stimulate a  $\Delta f'$  for one atom type may be unable to avoid or may deliberately seek to simultaneously have a  $\Delta f'$  for two or more atom types and that a cross-vector term occurs involving the two atom types (see Appendix 1 of Olczak *et al.*, 2003). Thus in such situations a Patterson map with coefficients  $(F_{LH\lambda_2} - F_{LH\lambda_1})^2$  would have self- and cross-vectors between the various anomalously scattering atom types and their constituent atom populations. This is unlikely to be a limiting situation in that, even with more than one anomalous scatterer type and each having more than one atom in each population, the total number of atoms sought from the Patterson is still very much less than that in the native Patterson, *i.e.* for the full structure, assuming that the cross-vectors to the light atoms are weak peaks.

As stated above, the resolution of the data can be truncated to 1.5 Å, greatly reducing the congestion of lines. From protein crystallography, it is known that relatively simple partial structures of the anomalous scatterers are derivable from diffraction resolutions significantly poorer than atomic resolution, either by Patterson or direct methods using anomalous differences (Mukherjee *et al.*, 1989).

On the theoretical basis, finally, mention must be made that a fundamental limitation of the powder method remains even with a two-wavelength approach; *i.e.* the hand of a molecule

cannot be determined because the Friedel equivalent reflections exactly coincide. In the protein case, it is known from the chemistry that, in nature, amino acids are left handed, this chemical property will be valuable in structure determination re choice of the hand.

### 3. Experimental

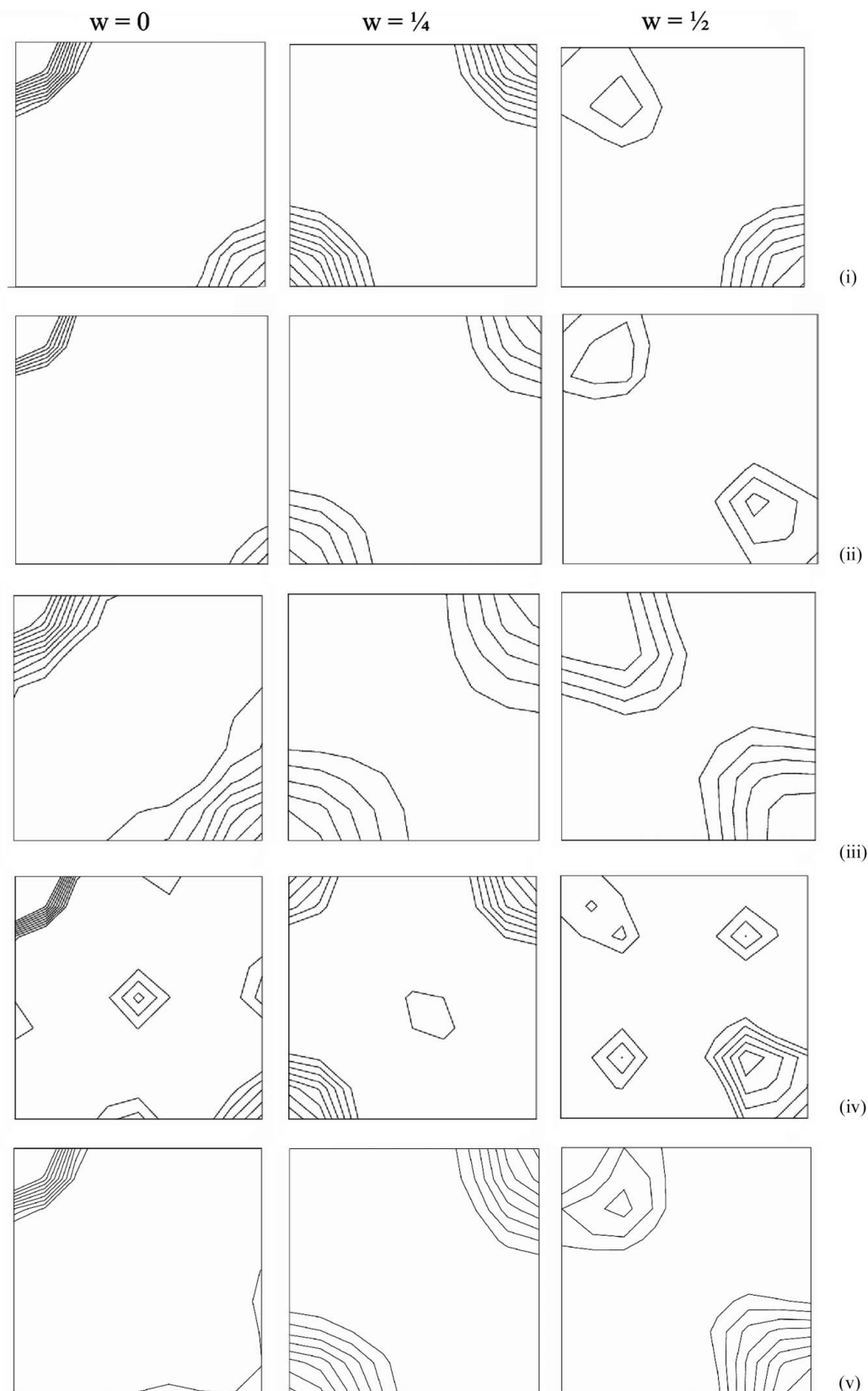
We have chosen a simple compound as a test case, namely nickel sulfate hexahydrate  $\text{Ni}(\text{SO}_4) \cdot 6(\text{H}_2\text{O})$ ; the Ni-atom *K* edge is well placed for SR source powder instrumentation usage, *i.e.* in the mid-X-ray wavelength range, to allow reference test data sets to be collected at shorter and longer wavelengths. This compound crystallizes in the tetragonal space group  $P4_12_12$  (No. 92) with  $a = 6.782$  and  $c = 18.274$  Å.

The literature value of the *K*-absorption edge of Ni is 1.4878 Å; the position is expected to be shifted to higher energy for  $\text{Ni}^{2+}$  by a few eV. The edge position of  $\text{NiSO}_4 \cdot 6\text{H}_2\text{O}$  was determined experimentally by fluorescence scans to be at 1.4889 Å, using the flat-plate mode, where the  $f'$  minimum was assumed to occur at a position half-way up the edge. (Note that the oxidation state of nickel is II and the edge position should be about 4 eV shifted to higher energy, *i.e.* shorter wavelength.) The value of 1.4889 Å contains an angular offset determined during calibration of the machine (Laundy *et al.*, 2003). Powder diffraction patterns were then collected in capillary mode. A redetermination of the *K*-edge position was made regularly at SRS reinjection, and subsequent absorption-edge determinations were carried out directly on the capillary mounted sample.

Powder diffraction data sets were collected at the  $f'$  dip at 1.4889 Å, the base of the edge at 1.4912 Å as well as at 1.7962 and 1.3002 Å, and finally at 2.1608 Å. The final wavelength values were determined by refining against the known lattice parameters for this compound for each data set (Rousseau *et al.*, 2000). Measurements were made to 120° in  $2\theta$ , except for the 2.1608 Å data, where data were collected to 130°  $2\theta$ . The data were corrected for beam decay using the incident-beam monitor. Data were extracted using the Le Bail method (Le Bail *et al.*, 1988) and using GSAS (Larson & Von Dreele, 1994) ( $\lambda = 1.4889$  Å,  $wR_p = 0.160$ ,  $R_p = 0.124$ ;  $\lambda = 1.4912$  Å,  $wR_p = 0.073$ ,  $R_p = 0.056$ ;  $\lambda = 1.7962$  Å,  $wR_p = 0.151$ ,  $R_p = 0.109$ ;  $\lambda = 1.3002$  Å,  $wR_p = 0.074$ ,  $R_p = 0.056$ ;  $\lambda = 2.1608$  Å,  $wR_p = 0.250$ ,  $R_p = 0.192$ ). In order to obtain a common scaling for all the data, the total number of counts ( $F_o^2$ ) for the first 278 extracted reflections was summed, except for the 2.1608 Å data set, which used the first 185 reflections. Initial scale factors were computed to give each data set the same number of counts and applied accordingly. For the data set measured at  $\lambda = 1.4912$  Å, the scale factor was set to one.

### 4. Analyses of the data sets

The  $w = 0$ ,  $w = \frac{1}{4}$  and  $w = \frac{1}{2}$  sections of the dispersive difference Patterson maps provide discrimination between the various wavelength pairs assessed, since these should have the strongest Ni–Ni vectors, at  $\frac{1}{2}$ , 0.08,  $\frac{1}{4}$  and 0.42 0.42,  $\frac{1}{2}$ , as well as

**Figure 2**

Comparison of dispersive difference Patterson sections  $w = 0$ ,  $w = \frac{1}{4}$  and  $w = \frac{1}{2}$  for (i)  $f'_{\text{dip}} - 1.8 \text{ \AA}$ , (ii)  $f'_{\text{dip}} - 1.3 \text{ \AA}$ , (iii)  $f'_{\text{dip}} - f'_{\text{base}}$ , (iv)  $f'_{\text{dip}} - 2.16 \text{ \AA}$ , (v) calculated  $f'_{\text{dip}} - 1.8 \text{ \AA}$ . The contour baseline was based on inspection of the maximum  $\rho$  values away from the origin peak and from Harker sections and thus was an estimation of the noise level for each wavelength pair. The contour interval was 10% of the maximum peak heights in the Harker sections for each wavelength pair.

**Table 1**

Details of the Patterson self- and cross-vectors for NiSO<sub>4</sub>·6H<sub>2</sub>O.

(a) The coordinates of the atoms in NiSO<sub>4</sub>·6H<sub>2</sub>O.

Atom	Position (fractional coordinates)
Ni	0.71, 0.71, 0
S	0.21, 0.21, 0
O1	0.11, 0.12, 0.07
O2	0.44, 0.17, 0.00
O3	0.67, 0.45, 0.06
O4	-0.03, 0.75, 0.06
O5	0.55, 0.85, 0.08

(b) The Patterson peak positions for the interatomic vectors in NiSO<sub>4</sub>·6H<sub>2</sub>O (the Patterson symmetry is *P4/mmm*).

Harker vectors <i>u, v, w</i>	Expected values for Ni	Expected values for S
2 <i>x</i> , 2 <i>y</i> , $\frac{1}{2}$	1.42, 1.42, $\frac{1}{2}$	0.42, 0.42, $\frac{1}{2}$
$\frac{1}{2}$ , 2 <i>y</i> + $\frac{1}{2}$ , 2 <i>z</i> + $\frac{1}{4}$	$\frac{1}{2}$ , 1.92, $\frac{1}{4}$	$\frac{1}{2}$ , 0.92, $\frac{1}{4}$
2 <i>y</i> , 2 <i>x</i> , $\frac{1}{2}$	1.42, 1.42, $\frac{1}{2}$	0.42, 0.42, $\frac{1}{2}$
$\frac{1}{2}$ , 2 <i>x</i> + $\frac{1}{2}$ , 2 <i>z</i> - $\frac{1}{4}$	$\frac{1}{2}$ , 1.92, - $\frac{1}{4}$	$\frac{1}{2}$ , 0.92, - $\frac{1}{4}$

Cross peaks	Position ( <i>u, v, w</i> )
Ni-S	0.5, 0.5, 0
	0.92, 0.92, $\frac{1}{2}$
Ni-O1	0.60, 0.59, -0.07
Ni-O2	0.27, 0.54, 0
Ni-O3	0.04, 0.26, -0.06
Ni-O4	0.68, -0.04, -0.06
Ni-O5	0.16, -0.14, -0.08

the weaker vectors owing to Ni-S at 0.5, 0.5, 0 and 0.08, 0.08,  $\frac{1}{2}$  (Table 1). The calculated peak heights for each interatomic vector have been assessed by comparison with the ‘native’ structure calculated Patterson ‘by inspection’.

In order to calculate these maps, it was necessary to place each data set on a common scale and this was carried out in two steps. Firstly, account of the SRS ring current decay was applied from ion chamber readings, as referred to above. The patterns simply scaled for beam current decay are given in the supplementary figures (as Le Bail extractions);<sup>1</sup> these do show directly changes in reflection intensities and by comparison of the calculated reflection intensities that are particularly sensitive to the Ni-atom changes in intensity can be ascribed to the differences in the Ni-atom *f'* at the various wavelengths. Secondly, use of the CCP4 program *SCALEIT* (Collaborative Computational Project, Number 4, 1994) option of isotropic scaling *versus* diffraction resolution was harnessed. This second scaling step yielded the best quality dispersive difference Patterson maps in terms of (i) a better correspondence of the expected Harker peaks and (ii) fewer noise peaks.

Fig. 2 compares these difference Patterson maps between the data measured at 1.4889 Å and other wavelengths, and with the calculated *f'* dispersive difference Patterson map.

<sup>1</sup> Figures showing plots of observed, calculated and difference patterns for Le Bail extractions versus *d* spacings, and dispersive Patterson maps for the non-CCP4 scaled data are available from the IUCr electronic archives (Reference: SH5034). Services for accessing these data are described at the back of the journal.

**Table 2**

Values of *f'* at the various wavelengths.

The refined values were obtained using GSAS; the value at 2.1608 Å used data truncated at 1.506 Å resolution. The calculated values are from Sasaki (1989).

λ (Å)	<i>f'</i> (refined) (e)	<i>f'</i> (calc.) (e)
1.4889	-7.361	-12.025
1.4912	-6.565	-6.272
1.7962	-2.253	-1.597
1.3002	-1.319	-1.071
2.1608	-0.064	-1.074

Table 1 shows the positions, in terms of *u, v* and *w*, of the peaks expected from the known crystal structure of NiSO<sub>4</sub>·6H<sub>2</sub>O, which shows, in particular, that the Ni-Ni vectors are coincident with the S-S vectors. However, the Ni-S cross-vectors should be much diminished in the dispersive difference Patterson; thus the best dispersive Patterson map is the (*f'* dip - 1.8 Å), *i.e.* Fig. 2(i). Besides the 1.8 Å reference wavelength set, the other candidate reference sets at 1.3 and 2.16 Å wavelengths also show good (*f'*<sub>dip</sub> - *f'*<sub>ref</sub>) Patterson sections, where *f'*<sub>ref</sub> is the value of *f'* at one of the reference wavelengths (1.3, 1.8 or 2.16 Å), but are somewhat noisier and have less diminished cross-vector peaks. The 1.3 Å wavelength data set was weak in average intensity owing to the SRS bending magnet λ<sub>c</sub> ≈ 4 Å. The 2.16 Å wavelength data set was weak owing to increased X-ray absorption in the Be windows and in the air path in the powder diffraction camera. The dispersive Patterson maps for the non-CCP4 scaled data in the supplementary material show that the best wavelength difference was for the (*f'*<sub>dip</sub> - *f'*<sub>base</sub>) pair, where *f'*<sub>base</sub> is the value of *f'* at the base of the Ni *K*-absorption edge, *i.e.* compare Fig. 2(iii) with Supplementary Fig. 2(iii). This is likely to be the optimum pair where a further scaling procedure is not needed; this could be a significant point to guide which immediate analyses to make ‘at the beamline’.

Refinement of the structure was carried out using *SHELXL97* (Sheldrick, 1997) and the starting Ni-atom position. This showed that the data were reasonably accurate to 1.5 Å resolution and also those data sets that were collected using multiple scans were the most precise. In order to confirm that the values obtained from the data for *f'* were reasonable, conventional Rietveld refinements were performed using GSAS (Larson & Von Dreele, 1994). The values of *f'* and *f''* for Ni, S and O atoms were initially set at their theoretical values. Then the positions and temperature factors of the atoms were allowed to refine as was the value of *f'* for the Ni atom. Table 2 shows the refined and calculated values of *f'* for the Ni atom at the various wavelengths, showing that the refined values for *f'* agree reasonably closely with the expected values.

The anomalous-scattering tables (Sasaki, 1989) show that the calculated minimum is at a wavelength of 1.4878 Å for a sampling interval of the calculation used of 0.0001 Å. Our value quoted here of 1.4889 Å is, as explained earlier in the text, subject to a calibration offset but is the *f'* dip position in fact. A wavelength shift of 0.0023 Å from 1.4889 to 1.4912 Å

allows simple interpolation to the second calculated value tabled here of  $-6.272$  e (from  $-12.025$  e). The refined value of  $-7.361$  e is not as negative as we would anticipate owing presumably to smearing factors of the instrument and limitations of the Rietveld approach.

A particular interest is the experience with the longest-wavelength data set recorded, *i.e.* at  $2.16$  Å wavelength. We refined against the  $2.16$  Å data. The data set has the worst data statistics, with  $wR_p = 0.250$ ,  $R_p = 0.192$ . This is reflected in the refined values of  $f'$  obtained when using all the data range, which was  $-4.591$  e; this is greater than that at  $1.8$  Å wavelength. The other problematic feature was that, whereas in all the other data sets  $U_{\text{iso}}$  was positive for all atoms, this was not the case for the Ni atom here where the  $U_{\text{iso}}$  became negative. These problems can be traced to the data collection being based simply on repeat scans. So whilst the signal to noise at low angles is good, the reflections at high angle are worse. However, a further refinement was carried out using the  $2.16$  Å wavelength data set but truncating the data at a resolution of  $1.506$  Å. This refinement led to a refined  $f'$  value of  $-0.064$  e, which is much closer to the theoretical value of  $-1.074$  e; in addition, all the isotropic temperature factors remained positive.

## 5. Discussion and conclusions

The choice of  $\text{Ni}(\text{SO}_4) \cdot 6\text{H}_2\text{O}$  had, as well as the benefits listed above, the complication that its space group was  $P4_12_12$ , which in an unknown case could have been  $P4_32_12$ , *i.e.* the enantiomeric space group. To resolve such a choice with PDD would require supplementary information such as prior chemical knowledge of the hand. In the protein case, the enantiopurity is known because all naturally occurring proteins are comprised of left-handed amino acids. There is then a potential limitation of PDD where the prior chemical knowledge is not available.

The additional *SCALEIT* data scaling used here proved to be helpful to the quality of the PDD Patterson maps. There are quite a few options that can be applied to optimize the signal extraction between the data sets at different wavelengths; we have explored one in detail here and it was successful. It was particularly interesting that the  $(f'_{\text{dip}} - f'_{\text{base}})$  pair, with its very small wavelength shift, gave good results without this additional data-set-to-data-set scaling. Scaling, however, might not work and this potential limitation needs to be explored in more detail and suitable protocols developed.

Our way of estimating the  $f'$  values gave quantitatively sensible results. Another way that is used is the Kramers-Kronig transform (KKT) (Evans & Pettifer, 1999).

We have explored the softer X-ray range here but of course we must mention its possible limitations. In particular, the increased absorption on the instrument, *e.g.* air paths, and in the sample, in effect, can reduce the signal and thereby the signal-to-noise ratio of the data, clearly not wished for. However, the core idea is that, for larger unit cells, the powder lines can be spread out by using softer X-rays. Of course, this

requires implicitly that the peaks individually do not widen more than the gain in their increased angular separation. This depends on the instrument and the sample of course but is generally true. A tunable undulator-based instrument, with its tiny divergence, has an ideal specification for exploring the relative gains and losses in the various wavelength range regimes of interest. Very recently, Cernik *et al.* (2005) have published details of powder diffraction pattern recording at a wavelength as long as  $5$  Å on an SRS bending magnet, and so longer wavelength experience is growing.

Overall, we have shown the following.

(i) The two wavelength-difference Patterson maps based on coefficients  $(F_{\text{LH}\lambda_2} - F_{\text{LH}\lambda_1})^2$  even where there is one Ni atom in the presence of a few light atoms for our test case yielded vectors dominated by the anomalous scatterer alone.

(ii) The Ni-atom position determined in (i) allowed difference Fourier cycling development of the rest of the structure from the anomalous-scatterer position using single-wavelength data.

(iii) The use of  $1.5$  Å resolution proved to be adequate for (i) and (ii).

(iv) The softer X-ray wavelength data-set-quality assessment had several problems with it; of especial note is the incorrect refined  $f'$  value. Improvements in data collection by using a helium path as well as our repeat-scans strategy is believed to be needed because of the already weak high-angle data being absorbed by air to make them too weak. The low-angle reflections suffered the same fate but were strong enough to give a reasonable signal-to-noise ratio. Pursuing this category of powder diffraction data collection we believe is important because it is a simple strategy to spread out the powder lines and it widens the  $\Delta f'$  range of values that can be stimulated for a variety of important elements like the transition metals in inorganic chemistry structural studies, halogens in pharmaceutical industry new drug discovery studies and sulfur, selenium, xenon or iodine in future protein crystallography powder analyses.

Overall, in our future synchrotron powder  $\Delta f'$  (PDD) experiments, we will explore extension to larger organic and inorganic structures than our test case where we believe that, in cases of a single anomalously scattering atom in the asymmetric unit of a crystal, the scope of *ab initio* structure solution from powder diffraction data can be considerably extended with our approach. Moreover, our PDD approach can be extended to proteins containing metal atoms, selenomethionine or perhaps even sulfur, and where one data set of the PDD group of data sets per study can harness the benefits of softer X-rays referred to above, *i.e.* especially spreading out the pattern but also increasing the sample scattering efficiency, which varies as  $\lambda^2$ . Especially exciting would be extending to yet smaller protein crystal samples, which would otherwise be outside the range of X-ray data collection from a protein microcrystal. In effect, in the protein powder case the sample volume is not restricted, unlike the protein single microcrystal case, offering a strategy for getting around sample X-radiation damage. The various experimental avenues and optimizations are quite numerous and will be investigated systematically.

We are grateful to C. C. Tang of SRS Daresbury for helpful advice on using SRS station 2.3.

### References

- Burger, K., Cox, D., Papoular, R. & Prandl, W. (1998). *J. Appl. Cryst.* **31**, 789–797.
- Cernik, R. J., Cheetham, A. K., Prout, C. K., Watkin, D. J., Wilkinson, A. P. & Willis, B. T. M. (1991). *J. Appl. Cryst.* **24**, 222–226.
- Cernik, R. J., Husheer, S., Smith, A. & Roper, M. (2005). *J. Synchrotron Rad.* **12**, 431–433.
- Collaborative Computational Project, Number 4 (1994). *Acta Cryst.* **D50**, 760–763.
- David, W. I. F., Shankland, K. & Shankland, N. (1998). *Chem. Commun.* pp. 931–932.
- Evans, G. & Pettifer, R. F. (2001). *J. Appl. Cryst.* **34**, 82–86.
- Gu, Y. X., Liu, Y. D., Hao, Q. & Fan, H. F. (2000). *Acta Cryst.* **A56**, 592–595.
- Harris, K. D. M., Tremayne, M., Lightfoot, P. & Bruce, P. G. (1994). *J. Am. Chem. Soc.* **116**, 3543–3547.
- Helliwell, J. R. (1992). *Macromolecular Crystallography with Synchrotron Radiation*. Cambridge University Press.
- Hendrickson, W. A., Horton, J. R. & Le Master, D. M. (1990). *EMBO J.* **9**, 1665–1672.
- Kariuki, B. M., Serrano-Gonzalez, H., Johnston, R. L. & Harris, K. D. M. (1997). *Chem. Phys. Lett.* **280**, 189–195.
- Larson, A. C. & Von Dreele, R. B. (1994). Los Alamos National Laboratory Report LAUR 86-748, Los Alamos, NM, USA.
- Laundy, D., Tang, C., Roberts, M., Miller, M., Thompson, S. & Bushnell-Wye, G. (2003). *J. Synchrotron Rad.* **10**, 183–186.
- Le Bail, A., Duroy, H. & Fourquet, J. L. (1988). *Mater. Res. Bull.* **23**, 447–452.
- Margiolaki, I., Wright, J. P., Fitch, A. N., Fox, G. C. & Von Dreele, R. B. (2005). *Acta Cryst.* **D61**, 423–432.
- Mitchell, C. M. (1957). *Acta Cryst.* **10**, 475–476.
- Mukherjee, A., Helliwell, J. R. & Main, P. (1989). *Acta Cryst.* **A45**, 715–718.
- Okaya, Y. & Pepinsky, R. (1956). *Phys. Rev.* **103**, 1645–1647.
- Olczak, A., Cianci, M., Hao, Q., Rizkallah, P. J., Raftery, J. & Helliwell, J. R. (2003). *Acta Cryst.* **A59**, 327–334.
- Pagola, S. & Stephens, P. W. (2000). *Mater. Sci. Forum*, **321–3**, 240–245.
- Prandl, W. (1990). *Acta Cryst.* **A46**, 988–992.
- Prandl, W. (1994). *Acta Cryst.* **A50**, 52–55.
- Ramakrishnan, V. & Biou, V. (1997). *Methods Enzymol.* **276**, 538–557.
- Rousseau, B., Maes, S. T. & Lenstra, A. T. H. (2000). *Acta Cryst.* **A56**, 300–307.
- Sasaki, S. (1989). KEK Report 88–14. National Laboratory for High Energy Physics, Tsukuba, Japan.
- Shankland, K., David, W. I. F. & Csoka, T. (1997). *Z. Kristallogr.* **212**, 550–552.
- Shankland, K., David, W. I. F. & Sivia, D. S. J. (1997). *Mater. Chem.* **7**, 569–572.
- Sheldrick, G. M. (1997). *SHELXL97. Program for Crystal Structure Refinement*. University of Göttingen, Germany.
- Tremayne, M., Kariuki, B. M. & Harris, K. D. M. (1997). *Angew. Chem. Int. Ed. Engl.* **36**, 770–772.
- Von Dreele, R. B., Stephens, P. W., Smith, G. D. & Blessing, R. H. (2000). *Acta Cryst.* **D56**, 1549–1553.
- Wood, I. G., Nicholls, L. & Brown, G. (1986). *J. Appl. Cryst.* **19**, 364–371.